

Miniaturization of step mirrors in a static Fourier transform spectrometer: theory and simulation

Cong Feng,^{1,2} Bo Wang,^{1,2} Zhongzhu Liang,^{1,3} and Jingqiu Liang^{1,4}

¹State Key Laboratory of Applied Optics, Changchun Institute of Optics, Fine Mechanics and Physics, Chinese Academy of Sciences, Changchun 130033, China

²Graduate School of Chinese Academy of Sciences, Beijing 100039, China

³e-mail: liangzz@ciomp.ac.cn

⁴e-mail: liangjq@ciomp.ac.cn

Received June 22, 2010; revised October 5, 2010; accepted November 3, 2010;
posted November 4, 2010 (Doc. ID 130530); published December 20, 2010

The diffraction at mirror facets restricts the size of step mirrors for static step-mirror-based Fourier transform spectrometers. This paper discusses the miniaturization of these step mirrors and proposes a quasiperiodic approximation of Fresnel diffraction to analyze the diffraction effect. Noise caused by diffraction is classified into approximation noise and edge noise. The edge-enlarge method is developed to reduce edge noise. This method can reduce mirror facet width to less than 30 times the longest wavelength to be studied. Simulation results are given. © 2010 Optical Society of America

OCIS codes: 300.6190, 300.6300, 050.1940.

1. INTRODUCTION

In recent years, with a growing need for real-time and small-platform spectrum detection, microspectrometers with lower resolving powers have been studied for such applications as environmental monitoring and process control. It is well known that a Fourier transform spectrometer (FTS) has broad applications in electromagnetic spectra due to high luminous flux and multichannel transmission capacity. Until now, many kinds of micro-optical electromechanical system (MOEMS) technology-based micro FTSs have been reported [1–7]. However, as most of the reported works are time modulated, movement precision and system stability are still big problems that limit MOEMS technology-based micro FTSs.

An interferometer without moving parts for Fourier transform spectroscopy was proposed by Linkemann *et al.* [8]. However, energy loss results from the sampling process. Moller discussed this problem and proposed a wavefront dividing interferometer based on Michelson's interferometer with flat mirrors replaced by step mirrors, which allows the obtaining of interferograms without a translation mechanism [9,10]. Institutions such as the Centre National d'Etudes Spatiales (CNES) in France [11–15] and EVI Research in Canada [16] have developed this kind of interferometer. Using MOEMS technology, a model of micro FTS [17] working in the visible and near-infrared band is also proposed. Compared with other micro FTS, it is spatially modulated and has the advantages of stability and simplified configuration. It also promises optical path differences (OPDs) with high precision, as MOEMS technology is used in manufacturing step mirrors [18]. In addition, because step heights can be accurately measured, the interpolation method can give regularly sampled signal values.

Molecular adherence technology allows 1000 mirror facets in a 100×100 mm surface [14], whereas MOEMS technology allows a mirror facet that is several hundred micrometers [18]. However, a disadvantage of this type of FTS is that diffraction exists at mirror facets. It becomes more and more serious as

wavelength increases and thus restricts the size of the step mirrors. According to Moller, the width of a facet should be more than 100 times the longest wavelength to be studied so that the diffraction effect would be negligible [9]. As wavelength gets to middle- or far-infrared, larger step mirrors are necessary; this brings disadvantages such as increased mass and volume. An imaging system is also needed before the detector to make an interferogram's size suitable for detection (for instance, the step mirror reflection surface in [15] is 80×100 mm, whereas the detector surface is 8×10 mm). So, for extending the working range to middle- or far-infrared without these disadvantages, it is necessary to explore how the step mirrors may be made as small as possible.

Here, the possibility of step mirror miniaturization is discussed. An approximation of Fresnel diffraction to analyze mirror facet diffraction is proposed along with modifying the spectrum to achieve real spectrum intensity. Noise is classified into approximation noise and edge noise. A method is developed to reduce the edge noise. This method can overcome diffraction restriction to the size of step mirrors in middle- and far-infrared. Simulation results are given.

2. PRINCIPLE OF THE STATIC FTS

Figure 1 shows the simplified configuration of the micro static FTS. The two step mirrors are core parts. Each step mirror has n steps. The total height of steps of the lower one is equal to one step height of the higher one. They are crossed to generate $n \times n$ beams with different OPDs. Each beam image in a corresponding section on the two-dimensional detector and interferometric intensity is recorded. $n \times n$ signal values are obtained and arranged after OPDs, then the average of these values (dc component) is subtracted to produce a "useful" value sequence (ac component). The spectrum is then reverted through Fourier transform.

If the width of the mirror facets is large enough to neglect diffraction, the interferometric intensity in a section is

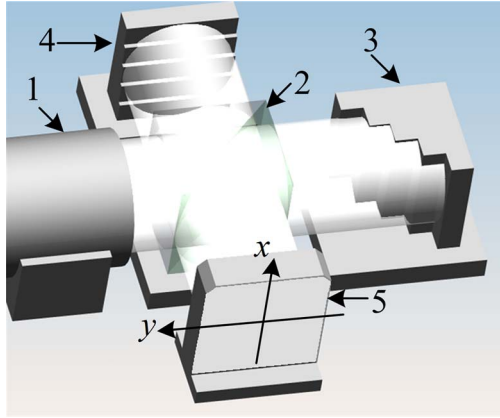


Fig. 1. (Color online) Simplified configuration of the micro static FTS. 1. Collimator. 2. Beam splitter (50% transmission, 50% reflection). 3. Higher step mirror. 4. Lower step mirror. 5. Two-dimensional detector. The coordinate system in the detector plane will be used in following discussion.

constant. Signal value should be integral of the intensity in this section:

$$V = IS = A(\sigma) + A(\sigma) \cos[4\pi\sigma(z_1 - z_2)], \quad (1)$$

where I is light intensity in this section, S is the area of the section, σ is the wavenumber, z_1 is the distance from the higher-step facets to the detector plane, and z_2 is from the lower one. $A(\sigma)$ is spectrum intensity, which can be obtained through Fourier transform.

3. THEORY DEVELOPMENT

A. Quasiperiodic Approximation

To analyze diffraction at facets, an approximation of Fresnel diffraction is necessary.

For Fresnel diffraction, the complex amplitude distribution function in sample plane is

$$U(x, y, z) = \frac{\exp(ikz)}{i\lambda z} \exp\left(ik \frac{x^2 + y^2}{2z}\right) \int_{-\infty}^{+\infty} \int_{-\infty}^{+\infty} U_0(x_1, y_1) \times \exp\left[ik \frac{(x_1^2 + y_1^2)}{2z}\right] \times \exp\left[-i \frac{2\pi}{\lambda z} (xx_1 + yy_1)\right] dx_1 dy_1, \quad (2)$$

where λ is wavelength, x, y are coordinates in the sample plane, x_1, y_1 are coordinates in the diffraction screen, and z is the distance between the sample plane and the diffraction screen, $k = 2\pi\sigma$.

If the width of the diffraction screen is much smaller than z , when z shift a little around a reference distance z_0 , only the factor $\exp(ikz)$ in Eq. (2) will change apparently. Equation (2) can be rewritten as

$$U(x, y, z) = A(x, y, z_0) \exp[i\phi(x, y, z_0)] \exp[ik(z - z_0)], \quad (3)$$

where $\phi(x, y, z_0)$ is a phase function, and $A(x, y, z_0)$ is amplitude. It shows a $k(z - z_0)$ phase shift in $U(x, y, z)$ compared with $U(x, y, z_0)$, which is called the quasiperiodic approximation.

The precision of this approximation depends on practical conditions, such as the transfer function of the diffraction screen, the intensity distribution of the light source, and the shape of the diffraction screen. Errors should be calculated before using this formula.

B. Analysis of Diffraction at Mirror Facets

Consider a single wavelength light source, and focus on a section that is not on the edge of the interferograms, which should leave the four nearest orthogonal sections around the chosen section.

The concern is for the beams' behaviors after diffraction. Each facet can be treated as a single rectangular hole through which parallel beams with different initial phases (caused by different facet depths) travel through, and sampled interferograms can be treated as a superposition of individual rectangular aperture diffractions. For a rectangular hole, the length is much larger than width; focusing on a section not on the edge, the complex amplitude distribution along the length can be neglected, and the rectangular aperture diffraction can be treated as a single slit diffraction. In this rectangular aperture diffraction model, z_0 is set to suit the requirement of the quasiperiodic approximation.

Now consider the complex amplitude distribution in this section (the middle one in Fig. 2). First, assume diffraction is not very strong, so that only the influence of these four sections should be considered.

Complex amplitude distribution function in this section can be written as

$$U'(x, y, z_1, z_2) = [U(y, z_1) + \exp(ikns)U(y - d, z_1 + ns) + \exp(-ikns)U(y + d, z_1 - ns)] \exp(ikz_1) \times \exp(-ikz_0) + [U(x, z_2) + \exp(iks) \times U(x - d, z_2 + s) + \exp(-iks)U(x + d, z_2 - s)] \times \exp(ikz_2) \exp(-ikz_0), \quad (4)$$

where n is the number of steps, d is the width of a facet, z_1 is the diffraction distance of the higher facet, z_2 is the diffraction distance of the lower one, and s is the step height of the lower step. $k = 2\pi\sigma$. $\exp(ikz_1)$, $\exp(ikz_2)$, $\exp(ikns)$, $\exp(-ikns)$, $\exp(iks)$, and $\exp(-iks)$ describe initial phases of beams from

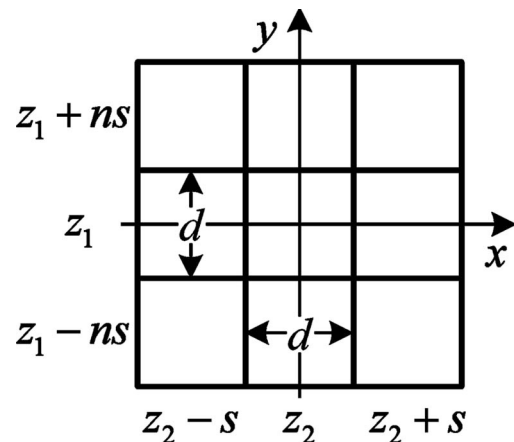


Fig. 2. Diffraction distances of different facets. Coordinate system is the same one shown in Fig. 1. Distances along y correspond to higher facets, and those along x correspond to lower ones.

different facets. $\exp(-ikz_0)$ is a constant introduced for the benefit of discussion. $U(x, z)$ or $U(y, z)$ stands for the complex amplitude distribution of a single slit diffraction with diffraction distance z . Equation (4) can be rewritten as Eq. (5) when quasiperiodic approximation is brought in:

$$\begin{aligned} U'(x, y, z_1, z_2) &= [U(y, z_0) + \exp(i2kns)U(y - d, z_0) \\ &\quad + \exp(-i2kns)U(y + d, z_0)] \exp[i2k(z_1 - z_0)] \\ &\quad + [U(x, z_0) + \exp(i2ks)U(x - d, z_0) \\ &\quad + \exp(-i2ks)U(x + d, z_0)] \exp[i2k(z_2 - z_0)] \\ &= B_1(y, z_0) \exp[i\phi_1(y, z_0)] \exp(i2kz_1) \\ &\quad + B_2(x, z_0) \exp[i\phi_2(x, z_0)] \exp(i2kz_2), \end{aligned} \quad (5)$$

where B_1 , B_2 , ϕ_1 , and ϕ_2 are constants determined by z_0 , x , and y . The corresponding signal value is integral of intensity

$$V(z_1, z_2, z_0) = \int_{-d/2}^{d/2} \int_{-d/2}^{d/2} U'(x, y, z_1, z_2) [U'(x, y, z_1, z_2)]^* dx dy. \quad (6)$$

It can be written as

$$V(z_1, z_2, z_0) = B + C \cos[2k(z_1 - z_2) + \theta], \quad (7)$$

in which

$$B = \int_{-d/2}^{d/2} \int_{-d/2}^{d/2} [B_1^2(y, z_0) + B_2^2(x, z_0)] dx dy, \quad (8)$$

$$\begin{aligned} C \exp(i\theta) &= 2 \int_{-d/2}^{d/2} \int_{-d/2}^{d/2} B_1(y, z_0) B_2(x, z_0) \\ &\quad \times \exp[i(\phi_1 - \phi_2)] dx dy. \end{aligned} \quad (9)$$

Comparing Eq. (8) with Eq. (9) gives

$$B \geq |C|, \quad (10)$$

which indicates a reduced fringe visibility. Then, $C(\sigma)$ is achieved through Fourier transform [$C(\sigma) = C$]. However, $C(\sigma)$ is not spectrum intensity, $A(\sigma)$ is. However, for fixed z_0 , d , s , the A/C values, which only vary with σ , can be calculated. So, A can be achieved by multiplying C by A/C .

If diffraction is negligible, $A/C \approx 1$. Modification to spectrum is not necessary; Eq. (7) returns to Eq. (1).

Equation (7) shows that the ‘‘OPD’’ of this section is no longer $2(z_1 - z_2)$, but, it seems to be, $2(z_1 - z_2) + \theta/k$. Actually, ‘‘OPD’’ is not logical here, as diffraction is playing an important part, and phase difference is not constant in the section. For the benefit of discussion, an ‘‘index optical path difference’’ (IOPD) is suggested, which is equal to the traditional concept of ‘‘OPD’’ here. For instance, the IOPD of this section is $2(z_1 - z_2)$.

If diffraction is very strong that more sections’ influences should be considered, the same formula can be obtained using the same method. For a continuous light source, as the interferogram is only the overlap of interferograms of different wavelengths, the discussion above is still valid.

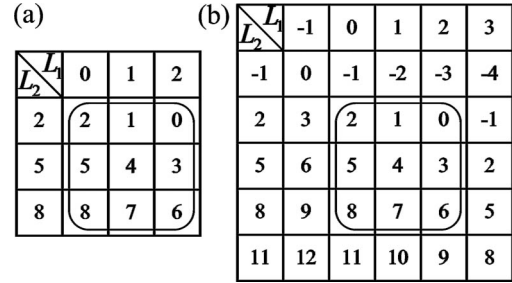


Fig. 3. (a) 3×3 sections, (b) 5×5 sections.

C. Edge-Enlarge Method

The discussion in Subsection 3.C is based on two assumptions:

1. quasiperiodic approximation,
2. the section is not on the edge so there are enough neighboring sections that surround it.

For sections on the edge, assumption 2, evidently, does not apply. Edge condition interrupts the applicability of the theory, and noise appears in the reverted spectrum. This is the edge noise, but noise is also caused by the precision of the quasiperiodic estimate of the approximation noise, the latter of which is usually negligible.

An edge-enlarge method is developed to eliminate the edge noise. Assume that diffraction is not very strong so that the influence of only the nearest sections needs to be considered. Let $n = 3$, which means three steps in each step mirror; this corresponds to 3×3 sections [Fig. 3(a)]. L_1 are the optical paths of beams from the lower step mirror with step height 1. L_2 are those from the higher step mirror with step height 3. The 3×3 sections in the rectangle with circular corners are sampled. The central section with IOPD 4 complies with the two assumptions above, but the others do not.

Adding one step to both sides of the step mirrors and lengthening each step to make 5×5 sections [Fig. 3(b)], the 3×3 sections in the rectangle with circular corners are still detected. As none of them are located on the edge, edge noise is eliminated.

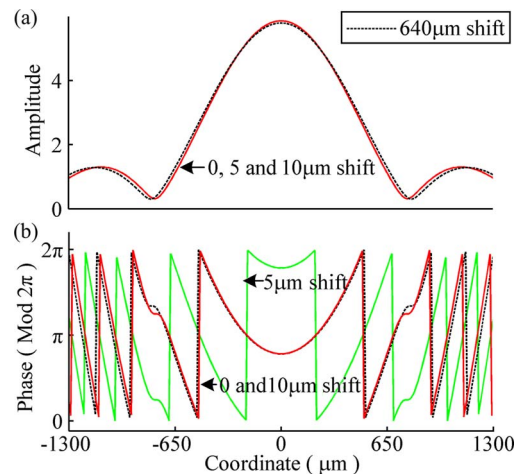


Fig. 4. (Color online) (a) Amplitude curves with 0, 5, 10 μm and 640 μm shift around z_0 , (b) corresponding phase curves.

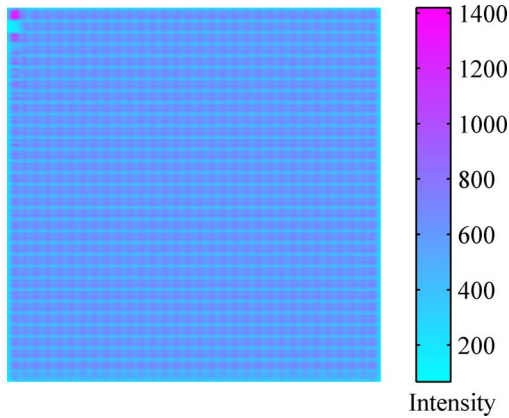


Fig. 5. (Color online) Interferogram of 32×32 steps for ideal blackbody radiation light source.

4. SIMULATION RESULT

The diffraction simulation code derived from the method discussed in the literature [19] was proved to be reliable by experimental results; the code herein obtained the same results as predicted.

The complex amplitude distribution on the detector plane for beams from each facet are calculated and summed to get the interferogram of one wavelength. Configuration parameters are set thus: the spectra wavelength range is $2.5\text{--}10\ \mu\text{m}$ (wavenumber, $0.1\text{--}0.4/\mu\text{m}$); according to the Nyquist sampling theorem, the lower step height is $0.625\ \mu\text{m}$; the width of a facet is $260\ \mu\text{m}$ (26 times the longest wavelength); the distance between the facet with $\text{OPD} = 0$ and the detector plane is 2 cm. A 32×32 interferogram is sampled, giving the largest OPD, $1278.75\ \mu\text{m}$ and 1024 signal values..

First, the precision of the quasiperiodic approximation, which is important for availability of the theory, is demonstrated. According to the discussion in Subsection 3.C, a single slit diffraction should be modeled: the width of the slit is $260\ \mu\text{m}$, and the wavelength is $10\ \mu\text{m}$. z_0 is 2 cm. Simulations with a 0, 5, and $10\ \mu\text{m}$ shift around z_0 are carried out. In Fig. 4(a), three amplitude curves cannot be distinguished, indicating the accuracy of amplitude approximation. Figure 4(b) shows the corresponding phase curves. Only two curves can be seen because the curves of z_0 and $z_0 + 10\ \mu\text{m}$ are superimposed on each other, indicating the accuracy of the phase shift

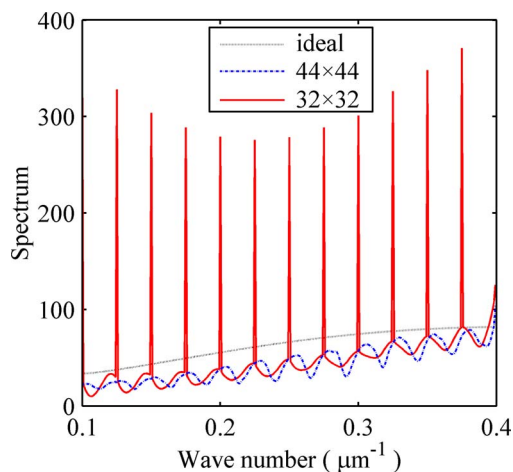


Fig. 6. (Color online) Spectrum reverted from 32×32 steps, 44×44 steps, and the ideal spectrum.

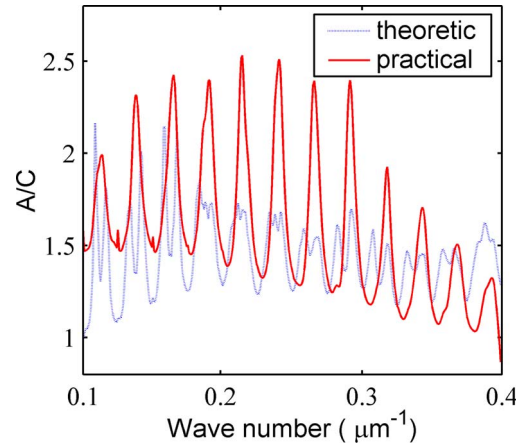


Fig. 7. (Color online) Theoretic and practical A/C values.

approximation. Calculate errors after a shift of $640\ \mu\text{m}$, which is a little longer than the longest shift of the facets. Results are also shown in Figs. 4(a) and 4(b). Compared with the diffraction at z_0 , the diffraction at $z_0 + 640\ \mu\text{m}$ shows an average error of 3.41% in amplitude and 2.42% in phase (calculating range, $-1300\text{--}1300\ \mu\text{m}$).

A. Result of the Edge-Enlarge Method for Continuous Light Source

The interferograms of an ideal blackbody radiation light source at a temperature of 1200 K are simulated.

Figure 5 shows an interferogram of 32×32 steps. The side effects at the interface of two sections caused by edges of facets as mentioned in [15] are also visible; however, pixels affected by this effect are still available as a result of the edge-enlarge method. Figure 6 shows the spectrum reverted from Fig. 5. Two other spectra in Fig. 6 are also plotted: the spectrum is reverted from 44×44 steps (12 steps added, six on both sides), and the ideal spectrum is reverted from the interferogram with diffraction totally neglected. The spectrum with 32×32 steps looks poor because of intense noise. As extra steps are added, the reverted spectrum slowly changes. After more than 44 steps, there will be no identifiable changes

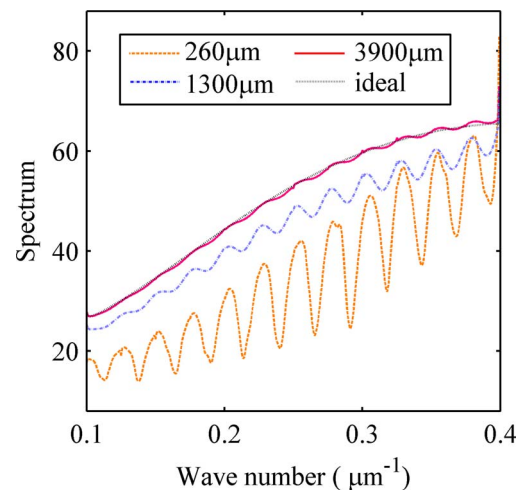


Fig. 8. (Color online) Diffraction-limited spectrum with facet widths 260, 1300, $3900\ \mu\text{m}$, and the ideal spectrum.

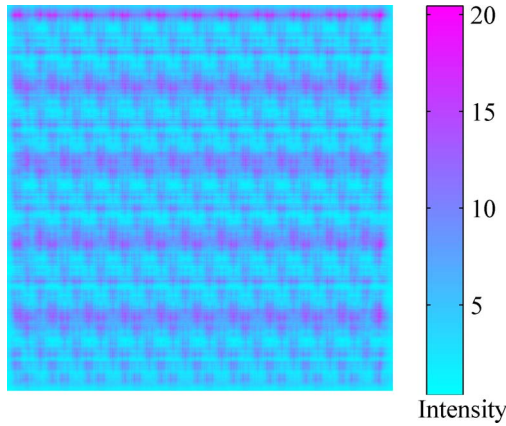


Fig. 9. (Color online) Interferograms of 32×32 steps for monochromatic light source.

in the spectrum, which is called the diffraction-limited spectrum.

Then, the A/C values are calculated using two different methods: the theoretic one is calculated following Eq. (9), and the practical one is calculated by dividing the ideal spectrum by the diffraction-limited one (see Fig. 7).

All theoretic A/C values are larger than 1. As wavenumbers increase, the A/C curve shows a slow downward trend to 1, which is logical as a result of the weaker diffraction effect. However, the practical A/C curve shows a significant difference. It also shows a faster downward trend to 1, but there is a stronger oscillation in this A/C curve. Further, there are values less than 1 near the wavenumber 0.4, indicating an impossible fringe visibility larger than 1 at corresponding wavenumbers. This is caused by the limited sample length and the rectangle apodizing function.

The reverted spectrum with the facets' widths of $1300 \mu\text{m}$ and $3900 \mu\text{m}$ are shown to clearly show diffraction's effect on the continuous spectrum (see Fig. 8). All spectra are reverted from 46×46 steps to ensure the diffraction-limited spectrum is obtained. As facet width increases, the reverted spectrum gets closer to the ideal one. Note that, even at $1300 \mu\text{m}$ (130 times the longest wavelength), the diffraction-limited spectrum still shows a significant difference from the ideal one. As the width increases to $3900 \mu\text{m}$, which is 390

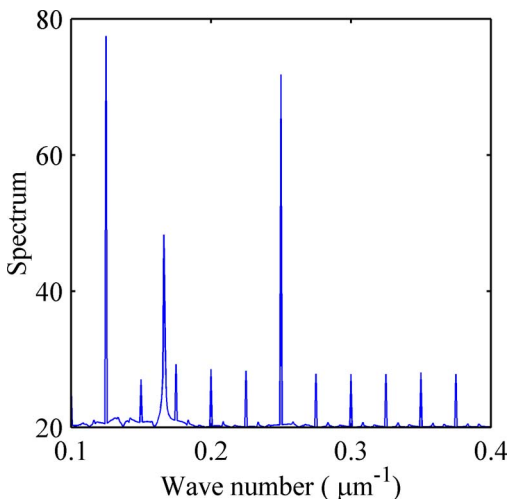


Fig. 10. (Color online) Spectrum reverted from 32×32 steps.

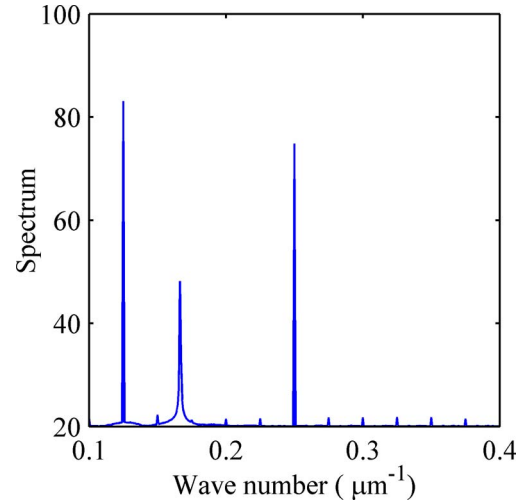


Fig. 11. (Color online) Spectrum reverted from 36×36 steps.

times the longest wavelength, the reverted spectrum appears to be very close to the ideal one.

The fringe visibility of an interferogram of 44×44 sections is 0.68. This is in accordance with Eq. (10). The entire reflection surface is $11.96 \times 11.96 \text{ mm}$ ($8.32 \times 8.32 \text{ mm}$ detected).

B. Result of the Edge-Enlarge Method for Discrete Light Source

In most practical cases, spectrometers are used to identify absorption or emission lines. Therefore, it is more important to identify absorption or emission lines in a reverted spectrum. For this reason, the system performance is simulated to a discrete light source.

A mix of three monochromatic light sources (wavelength of 4, 6, $8 \mu\text{m}$) is chosen as the incident beam. Figure 9 shows an interferogram of 32×32 steps. Figure 10 shows the corresponding reverted spectrum. Then, four steps are added to make a 36×36 interferogram. The reverted spectrum shown in Fig. 11 is much better than that in Fig. 10 as the noise here is depressed. It will be better if more steps are added.

For the purpose of identifying absorption or emission lines, four extra steps is enough. The fringe visibility of an interferogram of 36×36 steps is 0.625. This is also in accordance with Eq. (10). The entire reflection surface is $9.36 \times 9.36 \text{ mm}$ ($8.32 \times 8.32 \text{ mm}$ detected).

More steps should be added if narrower mirror facets are desired. However, the contrast decline should be considered.

At last, the signal-to-noise ratio (SNR) of the system is defined as

$$\text{SNR} = \frac{\int_{0.1}^{0.4} S_{\text{DL}}(\sigma) d\sigma}{\int_{0.1}^{0.4} |S_{\text{DL}}(\sigma) - S(\sigma)| d\sigma}, \quad (11)$$

where $S_{\text{DL}}(\sigma)$ is the diffraction-limited spectrum intensity, and $S(\sigma)$ is the spectrum intensity when different numbers of extra steps are added.

Table 1. SNR of the System with Different Numbers of Added Steps

Number of extra steps	0	2	4	6	8
Continuous light source	1.5	17.1	40.4	72.7	121.8
Discrete light source	1.5	5.2	19.0	29.6	31.7

Calculate the SNR with different numbers of added steps (see Table 1).

5. CONCLUSIONS AND DISCUSSION

In the proposed model, the precision of the quasiperiodic approximation depends on z_0 , d , s , which are decided by the shortest wavelength to be studied. It gets closer to periodicity with a larger z_0 and a smaller d , but this contributes little to the decrease of noise, as the edge noise will apparently increase.

When diffraction is considered, theory and simulation show that the fringe visibility of the interferogram will decrease. Two different criteria of fringe visibility were discussed in [16]; one is that the minimum fringe visibility over the entire detector area has to be more than a certain minimum value, such as 0.5. Simulation results show that this criterion can be well filled. As fringe visibility varies as a function of wavenumbers, it is necessary to modify the reverted spectrum with A/C values if one wants to obtain the real spectrum intensity. Two methods are discussed, and respective results are very different from each other. It is suggested that the practical A/C values are more suitable for a continuous spectrum modification.

Diffraction brings noise to the reverted spectrum. One may notice that an extremely large amount of noise appears at the wavenumbers of $(0.1 + n \times 0.025)/\mu\text{m}$ $n = 1, 2, 3, \dots$ in both Figs. 6 and 10. This is because for step mirrors with 32 steps, corresponding signal values are affected by the edge effect every 32 steps, which gives a typical wavelength of $2 \times 32 \times 0.625 = 40 \mu\text{m}$ (wavenumber $0.025/\mu\text{m}$). The simulation result shows that facets with a width more than 390 times the longest wavelength are more appropriate to render the diffraction effect negligible. When the diffraction effect is to be considered, noise caused by diffraction can be classified into approximation noise and edge noise. Approximation noise is usually negligible; as for edge noise, the edge-enlarge method is effective in decreasing it. This method can reduce mirror facet width to less than 30 times the longest wavelength to be studied, which brings many benefits, especially in the thermal infrared range.

ACKNOWLEDGMENTS

The authors are grateful to Dr. Jianguo Fu for his beneficial discussion of this manuscript and to Dr. Jinguang Lv and Dr. Ying Zheng for their help during this work. This work is supported by the National Natural Science Foundation of China (NSFC) under grants 60977062 and 61027010 and the National High Technology Research and Development Program (863) of China (grant 2009AA04Z315).

REFERENCES

1. S. H. Kong, D. D. L. Wijngaards, and R. F. Wolffenbuttel, "Infrared micro-spectrometer based on a diffraction grating," *Sens. Actuators A, Phys.* **92**, 88–95 (2001).
2. P.-P. Jiang, Y.-Q. Qiu, Z.-H. Fu, D.-Z. Yang, and Y.-H. Shen, "DSP and FPGA-based multi-channel fiber-optic spectrometer," *Opt. Precision Eng.* **14**, 944–948 (2006).
3. G. Lammel, S. Schweizer, and P. Renaud, "Microspectrometer based on a tunable optical filter of porous silicon," *Sens. Actuators A, Phys.* **92**, 52–59 (2001).
4. J. Sin, W. H. Lee, and D. Popa, "Assembled Fourier transform micro-spectrometer," *Proc. SPIE* **6109**, 610904 (2006).
5. K. Yu, D. Lee, U. Krishnamoorthy, N. Park, and O. Solgaard, "Micromachined Fourier transform spectrometer on silicon optical bench platform," *Sens. Actuators A, Phys.* **130–131**, 523–530 (2006).
6. U. Wallrabe, C. Solf, J. Mohr, and J. G. Korvink, "Miniaturized Fourier transform spectrometer for the near infrared wavelength regime incorporating an electromagnetic linear actuator," *Sens. Actuators A, Phys.* **123–124**, 459–467 (2005).
7. B. B. C. Kyotoku, L. Chen, and M. Lipson, "Sub-nm resolution cavity enhanced microspectrometer," *Opt. Express* **18**, 102–107 (2010).
8. J. Linkemann, F. Romero-Borja, and H. O. Tittel, "FT spectrometer with fixed mirrors using Fizeau fringes," *Proc. SPIE* **1575**, 184–187 (1992).
9. K. D. Moller, "Miniaturized wavefront-dividing interferometers without moving parts for field and space applications," *Proc. SPIE* **1992**, 130–139 (1993).
10. K. D. Moller, "Wave-front-dividing array interferometers without moving parts for real-time spectroscopy from the IR to the UV," *Appl. Opt.* **34**, 1493–1501 (1995).
11. J. Genest, P. Tremblay, and A. Villemare, "Throughput of tilted interferometers," *Appl. Opt.* **37**, 4819–4822 (1998).
12. A. Rosak and F. Tintó, "Progress report of a static Fourier transform spectrometer breadboard," in *Proceedings of the 5th International Conference on Space Optics* (ESA Publications Division, 2004), pp. 67–71.
13. F. Brachet, P.-J. Hébert, E. Cansot, C. Buil, A. Lacan, L. Roucayrol, E. Courau, F. Bernard, C. Casteras, J. Loesel, and C. Pierangelo, "Static Fourier transform spectroscopy breadboards for atmospheric chemistry and climate," *Proc. SPIE* **7100**, 710019 (2008).
14. C. Pierangelo, P. Hébert, C. Camy-Peyret, C. Clerbaux, P. Coheur, T. Phulpin, L. Lavanant, T. Tremas, P. Henry, and A. Rosak, "SIFTI: a Static Infrared Fourier Transform Interferometer dedicated to ozone and CO pollution monitoring," presented at the International TOVS Study Conference-16, Angra dos Reis, Brazil, 2008), post session B13.
15. A. Lacan, F.-M. Bréon, A. Rosak, F. Brachet, L. Roucayrol, P. Etcheto, C. Casteras, and Y. Salaün, "A static Fourier transform spectrometer for atmospheric sounding: concept and experimental implementation," *Opt. Express* **18**, 8311–8331 (2010).
16. E. V. Ivanov, "Static Fourier transform spectroscopy with enhanced resolving power," *J. Opt. A Pure Appl. Opt.* **2**, 519 (2000).
17. Y.-M. Kong, J.-Q. Liang, Z.-Z. Liang, B. Wang, and J. Zhang, "Micro assembled Fourier transform spectrometer," *Proc. SPIE* **7283**, 728304 (2009).
18. B. Wang, Z.-Z. Liang, Y.-M. Kong, J.-Q. Liang, J.-G. Fu, Z. Ying, W.-B. Zhu, J.-G. Lv, W.-B. Wang, P. Shu, and Z. Jun, "Design and fabrication of micro multi-mirrors based on silicon for micro-spectrometer," *Acta Phys. Sin.* **59**, 907–912 (2010).
19. G. Chengshan, L. Chuantao, H. Zhengping, and L. Tingting, "Suitability of different sampling methods for digital simulations of the optical diffraction," *Acta Opt. Sin.* **28**, 442–446 (2008).